ACS NANO
Cite This: ACS Nano 2018, 12, 7901−7910
www.acsnano.org

ARTICLE

Toughening Graphene by Integrating Carbon Nanotubes

Emily F. Hacopian,[†,○] Yingchao Yang,[‡,○] Bo Ni,[§,○] Yilun Li,[∥] Xing Li,[†,⊥] Qing Chen,[#] Hua Guo,[†] James M. Tour,[†,∥,▽] Huajian Gao,[§] and Jun Lou*[,†,∥]

[†]Department of Materials Science and NanoEngineering, Rice University, 6100 Main Street, Houston, Texas 77005, United States
[‡]Department of Mechanical Engineering, University of Maine, 5711 Boardman Hall, Orono, Maine 04469, United States
[§]School of Engineering, Brown University, 182 Hope Street, Providence, Rhode Island 02912, United States
[∥]Department of Chemistry, Rice University, 6100 Main Street, Houston, Texas 77005, United States
[⊥]Department of Physics and Engineering, Zhengzhou University, 75 Daxue Road, Zhengzhou 450052, China
[#]Key Laboratory for the Physics and Chemistry of Nanodevices and Department of Electronics, Peking University, Beijing 100871, P. R. China
[▽]NanoCarbon Center, Rice University, 6100 Main Street, Houston, Texas 77005, United States

Supporting Information

ABSTRACT: **Perfect graphene is believed to be one of the strongest materials, yet its resistance to fracture is much less impressive. The modest fracture toughness is thought to be related to the general brittle nature in the fracture process of graphene and its two-dimensional (2D) analogous. The brittleness also makes it extremely difficult to assess mechanical properties of 2D materials. The introduction of carbon nanotubes (CNTs) into bulk materials has proven to be a widely accepted method for toughening and strengthening materials. To date, such toughening effect of CNTs on 2D materials is largely unknown. A unique material, rebar graphene, has been synthesized that consists of CNTs embedded in graphene. In this study, by implementing a "dry" transfer technique, the freely suspended rebar graphene was systematically tested under uniaxial tension mode inside a scanning electron microscope. Our combined experiments and molecular dynamics simulations confirm that the embedded CNTs divert and bridge the propagating crack and provide a toughening mechanism for the material. Our work identifies a promising extrinsic toughening strategy for 2D materials and provides mechanistic insights into the fracture process of graphene hybrid material.**

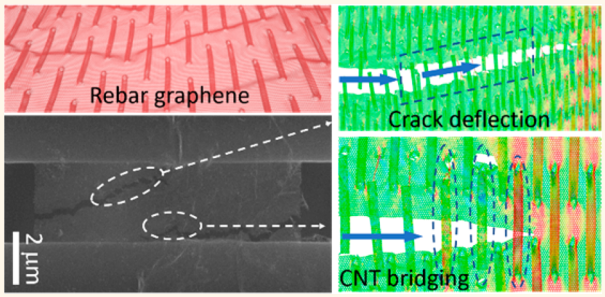

KEYWORDS: *rebar graphene, tensile test, fracture toughness, molecular dynamics, fracture behavior*

Following the discovery of graphene by Geim and co-workers, a lot of effort has been dedicated to better understanding the properties of graphene and its analogues.[1−10] Graphene has attracted huge attention due to its extraordinary properties, such as high electrical conductivity,[8,11] high intrinsic strength and Young's modulus,[12,13] and high thermal conductivity.[9,14] In perfect graphene, extremely high modulus and strength can be achieved under uniform stretching and breaking of the strong C−C bond.[2,5,7,13,15−18] However, like many other materials, defects are inevitable which weaken graphene considerably. Based on the Griffith theory, the strength of materials depends on the size of crack/flaw in materials, rather than the intrinsic strength. Fracture toughness, which characterizes a material's ability to resist fracture, is quite limited for graphene, as confirmed recently by both experiments and theoretical calculations. The previous study demonstrates that the fracture toughness of graphene is only 4.0 MPa·m$^{1/2}$,[1] which suggests that graphene is a typical brittle material. The magnitude of fracture toughness can not only determine the mechanical performance of materials but also strongly affect the reliability and stability of flexible devices built with those materials. Considering that graphene has a great potential in building flexible devices, in case of mechanical failure, graphene-like materials with higher fracture toughness are in need. It is thus very important to develop toughening strategies for this exciting material.

Received: March 27, 2018
Accepted: July 25, 2018
Published: July 27, 2018

DOI: 10.1021/acsnano.8b02311
ACS Nano 2018, 12, 7901−7910

Two general toughening strategies have been extensively explored in the past for bulk materials, namely, intrinsic toughening which exploits the microstructural features such as grain or phase structures to increase material toughness[6,19] or extrinsic toughening where additional material components are added to help retard the crack advancement and improve fracture resistance.[20,21] A representative example of extrinsic toughening is graphene reinforced nanocomposites. Due to its exceptional mechanical properties, high aspect ratio, and low density, graphene is an ideal candidate for developing the next generation of polymer-matrix, metal-matrix, and ceramic-matrix composites. To date, there has been a significant amount of research work with focus on graphene reinforced composites. The related composites include: randomly dispersed graphene into matrix to reinforce composites;[22,23] functionalized graphene to reinforce composites;[24,25] laminated graphene or graphene oxide to reinforce composites;[26] three-dimensional (3D) graphene foams to reinforce composites;[27] hybrid graphene and other nanostructures to reinforce composites.[28] Since it is still quite challenging to precisely control the microstructural features such as grain structures in graphene and there exists only limited evidence of sufficiently strong interactions between grain boundaries and crack tips in graphene, extrinsic toughening strategy seems to be a more plausible choice to toughen graphene.[17,29]

Because of the weak van der Waals interaction between 2D layers giving rise to rather inert surfaces that are free of dangling bonds, ideas have long been sought to engineer graphene properties through integration with other 2D materials. One such example is the so-called "van der Waals solid",[30] where graphene has been layered with various 2D materials to create vertical heterostructures exhibiting unique properties for electronic and optoelectronic applications.[10,30,31] However, the inertness of the 2D material surface makes it more difficult for effective load transfer between layers that is oftentimes necessary for desired enhancement of mechanical properties as sought after in this study. Alternative strategies are clearly needed to fulfill the goal of toughening graphene. Yan *et al.* has pioneered the synthesis of a new graphene hybrid material that combines a one-dimensional (1D) material, carbon nanotubes (CNTs), and a 2D material, graphene, into an integrated material.[4,32] This concept of the so-called "rebar graphene" nicely relates the macroscopic idea of using embedded reinforcing steel bars to toughen and strengthen concrete to a 2D material in nanoscale. Many studies have been performed on the integration of CNTs into bulk materials, such as metals, polymers, and ceramics, to make nanocomposites with enhanced mechanical properties.[33,34] However, research on the mechanical interaction of CNTs with layered 2D materials is sparse.[35]

In this study, we systematically investigated fracture behaviors of the freely suspended rebar graphene under uniaxial tension mode inside a scanning electron microscope (SEM). Our combined experiments and molecular dynamics (MD) simulations confirm that the embedded CNTs divert and bridge the propagating crack and provide a toughening mechanism for the material.

RESULTS AND DISCUSSION

Figure 1a provides a schematic illustration of rebar graphene and illustrates how CNTs are embedded into monolayer polycrystalline graphene. Rebar graphene is characterized using Raman spectroscopy as shown in Figure 1b. A 514 nm

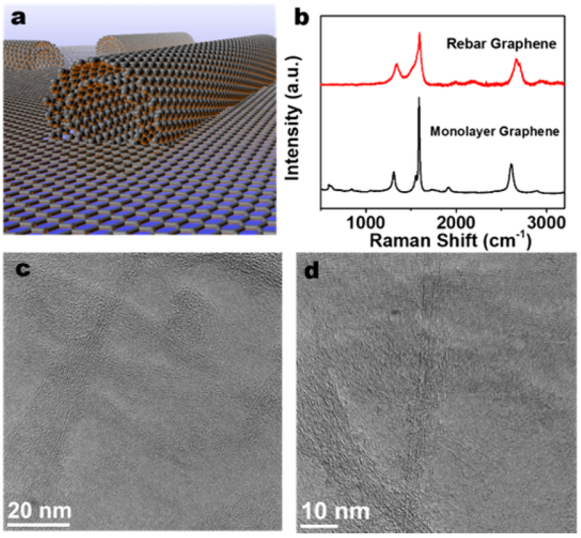

Figure 1. Rebar graphene characterizations. (a) Schematic illustration of rebar graphene. (b) Raman spectra. (c–d) High-resolution TEM images of rebar graphene.

excitation was used on rebar graphene and graphene, both on Cu foils in 10 different areas of a 1 cm^2 sample size. The Raman spectra of graphene exhibit two key features: a G peak at ~1580 cm^{-1} and a G′ or 2D peak at ~2700 cm^{-1}. The D peak at ~1350 cm^{-1} correlates with the presence of some sp^3 carbon atoms or defects. The rebar graphene spectrum has a shoulder on the 2D peak at ~2698 cm^{-1}, similar to monolayer graphene on copper. This shoulder location suggests a dominance of monolayer graphene in the rebar graphene sheets. Further characterization is seen in transmission electron microscopy (TEM) where the CNTs are shown in Figure 1d,e. The images illustrate the interconnected CNT networks on graphene sheets. TEM images also reveal that some regions of the rebar graphene sample might have two-layer graphene islands, however the Raman spectra suggest a strong dominance of monolayer graphene. Based on the growth method and previous study, it is believed that CNTs are packed on the top of graphene layer, instead of forming a sandwiched 3D network on both sides of graphene.[4]

One of the biggest challenges in quantitatively characterizing mechanical properties of 2D materials is proper sample preparations. Transferring 2D materials requires spin coating a polymer, such as poly(methyl methacrylate) (PMMA), to provide support during handling. Typically, these polymers can be removed using acetone; however, the suspended working layer of the mechanical device used for the tensile test of nanomaterials requires a dry transfer technique that avoids the use of any liquid, as shown in Figure 2a–d.[3] The process starts with spin coating a PMMA layer about 200–300 nm thick on the as-grown rebar graphene on copper substrate. The substrate is etched away, and a floating layer of rebar graphene and PMMA is left and fished out with a silicon substrate. After extensive washing, the film is transferred onto a TEM grid. The TEM grid is used to mitigate contact between the film and the substrate and add ease to the process of removing the film from the substrate. Under an optical microscope, a fine-tungsten probe is used to cut away the area of the material that will be tested. The same probe is used to gently place the rebar graphene/PMMA on the test section of the micromechanical testing device. Once contact between the film and device is

DOI: 10.1021/acsnano.8b02311
ACS Nano 2018, 12, 7901–7910

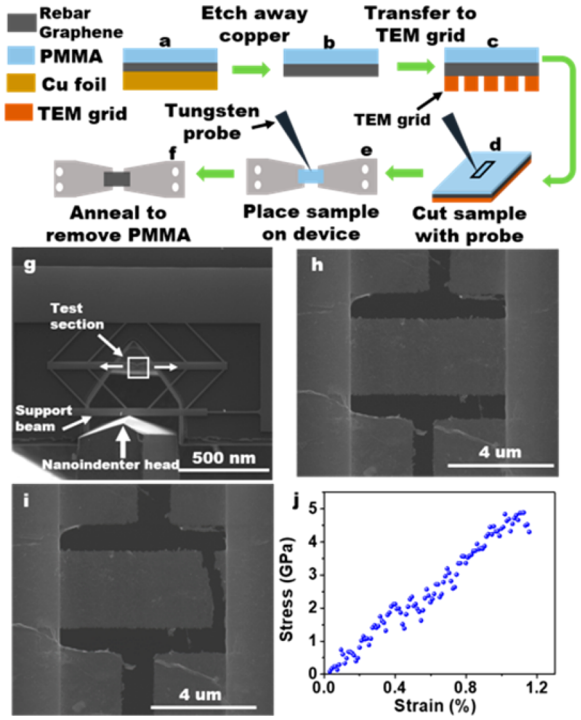

Figure 2. Sample preparation and testing results. (a–d) After spin coating PMMA on rebar graphene sample, the copper substrate is etched away, and a tungsten probe is used to cut out the sample area under optical microscope. (e) The sample area is placed in test section of the micromechanical device. (f) The devices are annealed in a CVD furnace with N_2/H_2 mixture to remove PMMA. (g) SEM image of the testing device geometry. (h) SEM image of film in test area of device before fracture. (i) SEM image of film in test area after fracture to show the zigzag fracture surface. (j) Stress–strain curve of the sample depicted in previous two images.

made, heat treatment is used to ensure proper adhesion. The entire device with the attached film is placed in a tube furnace and annealed under flow of hydrogen and nitrogen to remove the PMMA coating and leave the rebar graphene in the test section. The suspended rebar graphene is cut into a rectangular geometry using a focused ion beam (FIB). Careful attention is paid to use a beam current of <40 pA to protect the integrity of the suspended material. Figure 2h provides a depiction of the rectangular geometry for ease of calculation in data processing. The device, pictured in Figure 2g, exercises a spring-like "push–pull" mechanism and is actuated *in situ* by an Agilent nanoindenter to quantify the mechanical properties of 2D materials, including rebar graphene.[1,3] The indenter provides measurements of load and displacement, and the tests are video recorded to understand crack propagation. In 1D material tensile tests, platinum deposition is required to adhere the sample to the test shuttles.[36,37] Fortunately, to prevent sliding during tests of 2D materials, no additional deposition of platinum or epoxy is needed because 2D materials adhere to the test shuttle surface by van der Waals forces.[1,3] The stress–strain relationship for the sample depicted in Figure 2h,I is shown in Figure 2j. The stress–strain relationship exhibits a linear slope, corresponding to an elastic regime, and an abrupt ending, corresponding to the fracture of the sample. The rebar graphene samples fracture leading to a zigzag type fracture surface.

Evidence of a zigzag crack propagation of rebar graphene is presented in Figure 3. This fracture surface is due to the CNTs redirecting the motion of the crack and guiding the propagation in a zigzag formation. Pristine graphene fractures in a very linear crack down the center of the sample, as shown in the study by Zhang *et al.*[1] Graphene alone is brittle and exhibits a direct fracture, but rebar graphene shows a fracture pattern that has been stopped and redirected by CNTs. The longer length of the rebar graphene fracture surface compared to that of graphene indicates a higher fracture energy consumption in the rebar graphene samples.

To gain a better understanding of the toughening effects of embedded CNTs on graphene, a series of fracture tests were performed to measure the critical stress intensity factor (SIF) of this unique material. A center notch, ~10% of the total sample width, was cut into the sample. The eq 1 below was used to calculate the critical SIF K_c:

$$K_c = \sigma_c\sqrt{\pi a_0} \tag{1}$$

where a_0 is the half notch length and σ_c is the fracture strength.

The modulus and fracture strength are presented in Table 1. The average modulus of the tested un-notched rebar graphene samples is 466.80 ± 91.49 GPa, and the average fracture strength of the notched samples is 6.02 ± 4.67 GPa. The ranges of fracture strength and elastic modulus of rebar graphene are slightly broad, which could result from small SWCNT bundles, holes, and residual stress in rebar graphene. Detailed discussion can be found in the Supporting Information. Another concern is that the thermal expansion of device shuttles could lead to large stress which would tear rebar graphene as well. Note that the thickness of 0.7 nm was

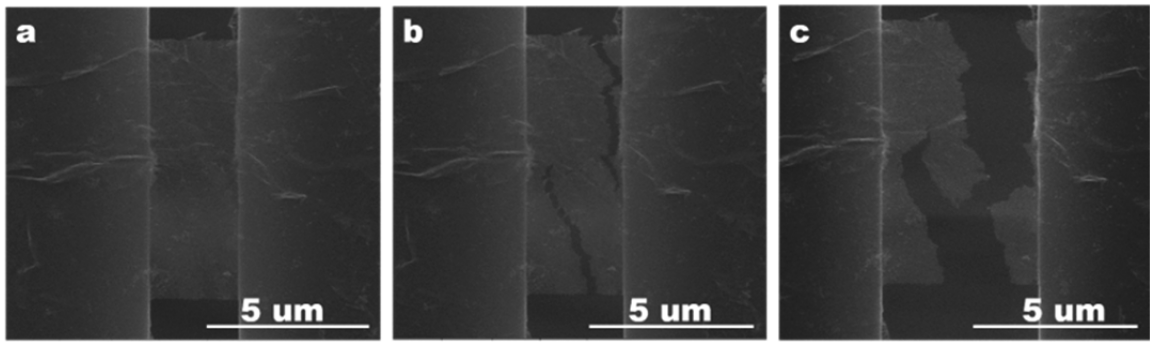

Figure 3. Crack propagation in rebar graphene. (a) Rebar graphene suspended over microdevice before loading. (b) Rebar graphene during tensile loading with zigzag crack propagation path and multiple crack formation. (c) Fractured rebar graphene showing rough fracture surfaces.

DOI: 10.1021/acsnano.8b02311
ACS Nano 2018, 12, 7901–7910

Table 1. Mechanical Properties of Suspended Rebar Graphene[a]

sample number	total strain (%)	Young's modulus (GPa)	fracture strength (GPa)
B1	1.16	431.69	4.89
B2	3.84	461.60	15.14
B3	0.65	490.97	2.86
B4	0.41	324.84	1.35
B5	2.30	415.95	6.92
B6	2.43	527.65	8.08
B7	2.36	614.90	2.93
average		466.80 ± 91.49	6.02 ± 4.67

[a]A measured average thickness of 0.7 nm is used here.

used to calculate the elastic modulus, fracture strength, and SIF of rebar graphene due to the nonuniformity of rebar graphene. More detailed discussions on the strength and stiffness of rebar graphene could be found in the Supporting Information. The SIF values determined by these experimental tests are presented in Table 2. In comparison to similar studies

Table 2. Geometry of Initial Crack Length with Respect to Total Sample Width Compared to Stress Intensity Factor As Calculated by the Griffith theory[a]

sample number	flaw ratio (%)	total strain (GPa)	fracture strength (GPa)	stress intensity factor ($MPa \cdot m^{1/2}$)
A1	8.53	1.33	5.08	7.23
A2	12.34	0.93	3.73	6.99
A3	15.92	2.13	2.41	4.43
A4	14.43	2.17	5.57	10.61
A5	38.09	4.65	2.65	8.30
A6	18.24	3.54	12.81	21.18
A7	13.58	2.01	9.00	14.75
average			5.89 ± 3.78	10.50 ± 5.73

[a]A measured average thickness of 0.7 nm is used here.

performed on pristine graphene, the average SIF of rebar graphene is clearly much higher. This can be explained by the ability of the CNTs to constrict and divert the propagation of the crack.

The *in situ* SEM tensile tests enable us to quantify the elastic modulus, fracture strength, and fracture toughness of rebar graphene. The critical SIF is over twice as much as that of graphene. To unveil the mystery behind the improved mechanical properties and to understand the interaction between CNTs and graphene as well as between the initial crack and CNTs, we performed *in situ* tensile tests of rebar graphene in TEM shown in Figure 4. A piece of rebar graphene was first transferred onto the TEM microdevice using the same transfer technique mentioned above. Figure 4a shows that the TEM image of rebar graphene firmly adhered to the TEM microdevice. The corresponding SEM image can be found in the Supporting Information Figure S1. There are several holes in the rebar graphene, which might have resulted from the dry transfer. However, the pre-existing holes can be considered an initial notch to observe crack propagation during the tensile test. The uniaxial tensile test was actuated by joule heating described in the Methods section. Figure 4b captures the moment of fracture of rebar graphene at which the crack went through the observed hole and was also greatly deflected. The crack deflection is desired for material toughening since more energy could be dissipated during the fracture process, leading to the enhancement of mechanical performance of rebar graphene. Figure 4c shows an overview of the fractured rebar graphene. Unlike fractured CVD grown graphene with a single straight crack line, there are several cracks in the fractured rebar graphene. This observation suggests multiple locations for crack initiation that inhibit the momentum of the primary crack driving force. Such phenomenon is also reflected by the different maximum strains between CVD grown graphene and rebar graphene. The maximum strain for CVD grown graphene is only 0.3%,[1] while the average maximum strain of rebar graphene is up to 1.5%. More fracture details in Figure 4d–f were investigated to understand the reinforcing mechanism. Some fractured shrinking tips of CNTs can be found in Figure 4e,f. The shrinking tips demonstrate that the CNTs bridged the crack growth before the catastrophic failure. The CNT bridging dominates the rebar graphene fracture surface, which successfully retard the crack growth in mechanical failure of rebar graphene shown in Figure 4e,f. The graphene bridging is also found in Figure 4e,f, complementing the enhancement of toughness of rebar graphene. In addition to the above reinforcing phenomena, the pulled-out CNTs can be observed around the fracture surface in Figure 4e,f, which is another reinforcing mechanism to improve the fracture toughness of materials. With the above observed reinforcing mechanisms, more energy could be consumed before final failure, which promotes the toughness of rebar graphene.

To further validate the hypothesized toughening mechanisms and unveil more details of the fracture process in rebar graphene, we have constructed full-atom models of rebar graphene with typical distributions of CNTs. MD simulations of crack propagation and uniaxial tension tests of rebar graphene nanostrips were carefully performed. The rebar graphene samples are built by connecting CNTs with a diameter of 1 nm and length of 11 nm to a graphene layer through sp^2 covalent bonds (Figure 5a). As the representative examples, only the CNTs lying along the vertical loading direction are presented here, and several typical CNT distribution patterns, including the regular staggered pattern, inclined staggered pattern, and random staggered pattern, are discussed, respectively (Figure 5b). More discussions about the effect of the varying geometry and distribution of CNTs on the toughness enhancement could be found in the Supporting Information.

After the full atomic arrangement of the rebar graphene structures are obtained, we performed MD simulations of relaxation and uniaxial tension in rebar graphene strips 200 nm in length and 100 nm in width, with/without a 50 nm long edge crack initially (Figure 5c). An initial relaxation under an NPT ensemble with Nose–Hoover thermostat[38] at 0 Pa and 300 K for 50 ps was performed first to make sure the rebar graphene models are thermodynamically stable. Then to perform the mechanical test, a tensile loading with a constant strain rate of 10^9 s^{-1} was applied by deforming the simulation box in the y direction. During the test, periodic boundary condition was applied in the y direction and an NVT ensemble with Nose–Hoover thermostat[38] was adopted to maintain a constant temperature of 10 K. Note that the length of the CNTs and the size of rebar graphene strips in these MD models are smaller than those of the experimental samples mainly due to the limitation of current simulation power. Nevertheless, it appears that the interaction between CNTs and graphene and the distribution of CNT network are

DOI: 10.1021/acsnano.8b02311
ACS Nano 2018, 12, 7901–7910

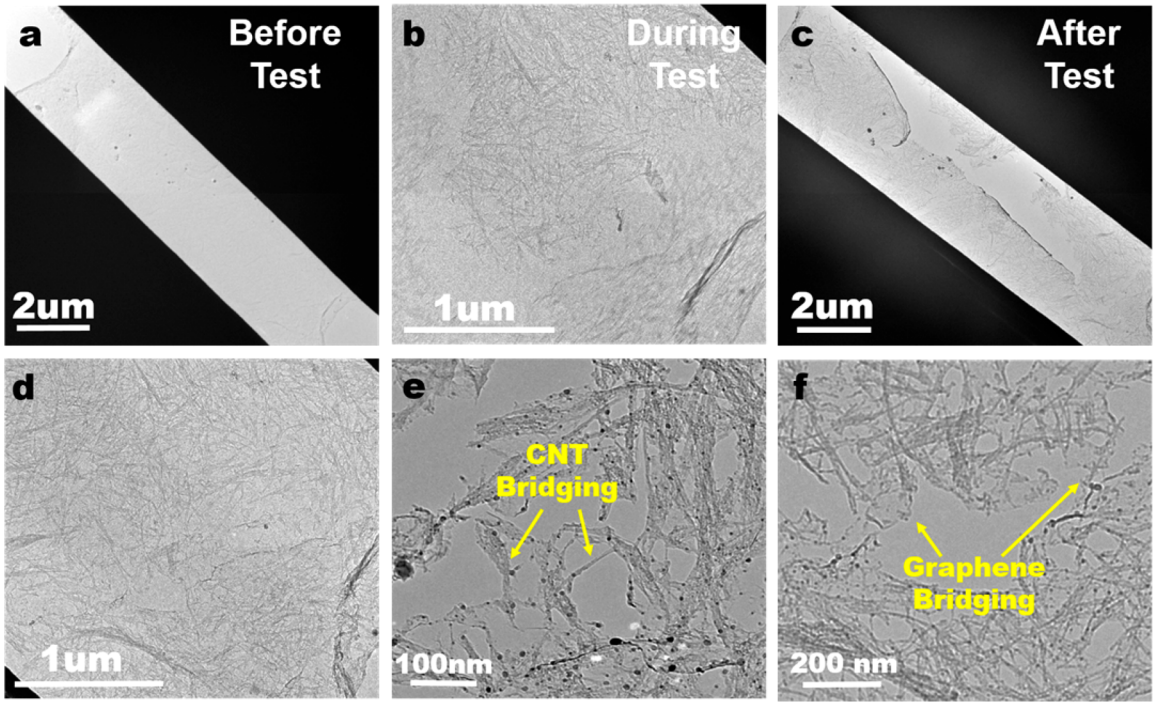

Figure 4. ***In situ*** **tensile test of rebar graphene in TEM. (a) Rebar graphene suspended over microdevice before tensile test. (b) Rebar graphene at the onset of fracture. (c) Overview of fractured rebar graphene. (d–f) Fractured rebar graphene with pulled-out CNTs, CNT bridging, and graphene bridging.**

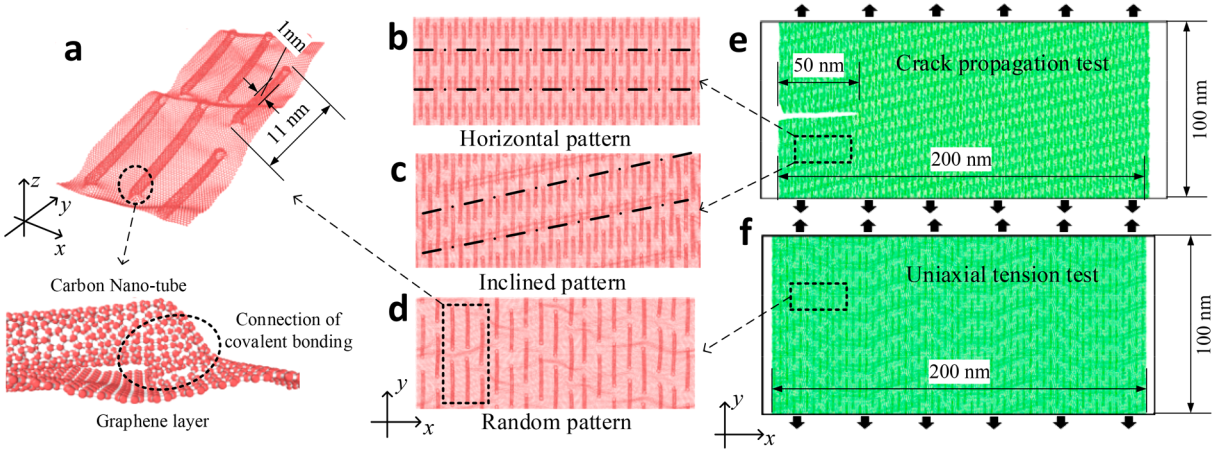

Figure 5. MD simulations of uniaxial tensile fracture tests of rebar graphene samples. (a) The atomic structure of rebar graphene samples. CNTs with a diameter of 1 nm and a length of 11 nm are connected to a graphene layer through sp^2 covalent bonds to represent rebar graphene samples. (b–d) Different distributions of reinforcing CNTs lying along the *y* direction. A regular staggered pattern (b), an inclined staggered pattern (c), and a random staggered pattern (d) are constructed. (e, f) MD simulations of crack propagation and uniaxial tension of rebar graphene nanostrips.

reasonably captured by the MD simulations, which prove to play key roles in achieving the observed toughening mechanisms in rebar graphene.

MD simulations of crack propagation were performed in rebar graphene samples (Figure 5e) to investigate the interaction between CNTs and crack. The results demonstrate that the crack could be bridged and/or deflected by CNTs in rebar graphene. Figure 6a shows that as the loading increases along the crack path, stress is transferred by the CNTs which bridge the two crack surfaces, postponing the main crack propagation. The crack propagates only when the bridging CNTs are broken or pulled out, leading to a strong bridging effect (Figure 6e) of the CNTs perpendicular to the initial crack path (see Movie S1 in Supporting Information). The ending of individual CNT bridging (Figure 6c) results from either the breaking of the CNT (Figure 6b) or the daughter crack initiation in the connected graphene layer (Figure 6d). These two localized, atomistic fracture events can be related to the local stress distribution and local atomistic configurations (*i.e.*, the topological defect structures). As shown in Figure 6g, when the CNT bridges the crack surfaces, high stress concentration builds up at the connection region between the CNT and the graphene layer. Locally, to accommodate the curvature change from the cylindrical CNT to flat graphene, there are positive and negative disclinations (pentagon and heptagon rings) at the connection spots. Previous studies have

DOI: 10.1021/acsnano.8b02311
ACS Nano 2018, 12, 7901–7910

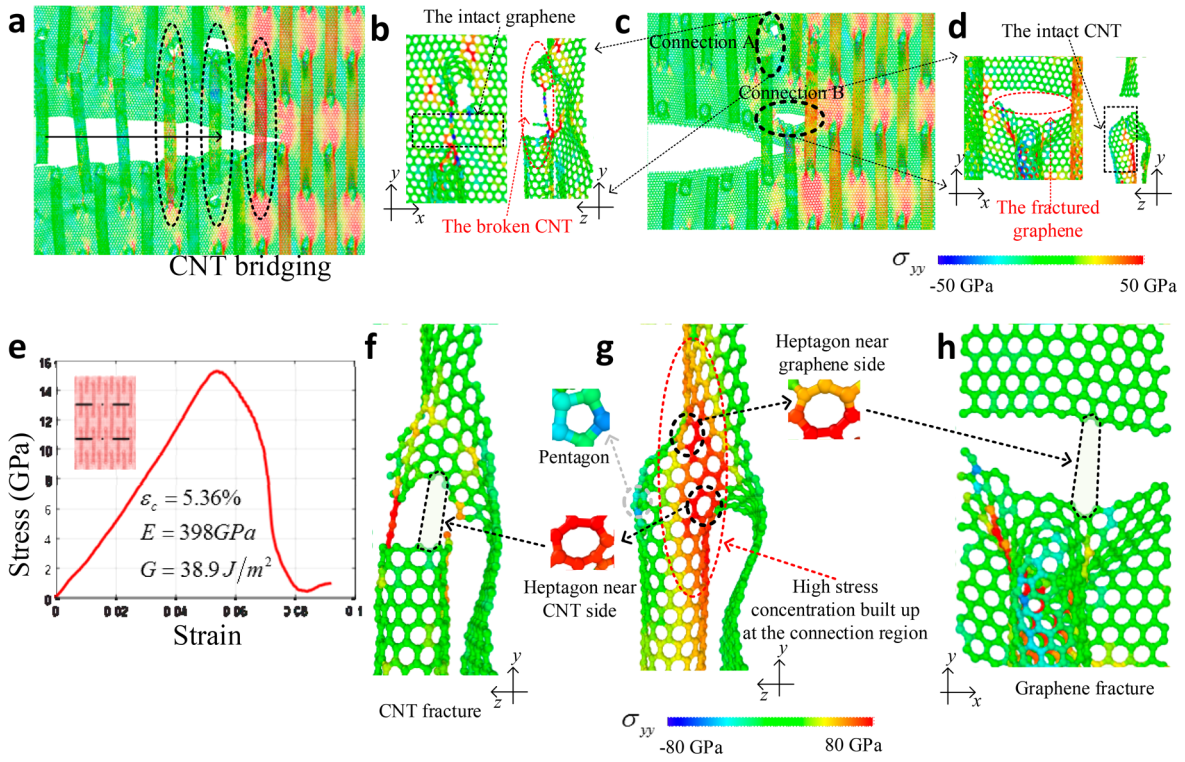

Figure 6. MD simulations of CNT bridging in rebar graphene samples. (a) MD simulation of crack propagation in a rebar graphene with CNTs in a regular staggered distribution pattern. The CNTs bridge the crack surfaces and fail as the crack propagates and the measured fracture toughness is enhanced. (b–d) Two failure modes of the bridging CNTs. The CNT could break leaving the graphene layer intact (top view and side view shown in b), or the graphene layer fractures with the CNT unbroken (top view and side view shown in d). (e) The stress–strain curve of the crack propagation test in a rebar graphene with CNTs in a regular staggered distribution pattern. The measured fracture energy, *G*, is 38.9 J/m^2, larger than that of graphene, 11.9 J/m^2, obtained *via* MD simulations. (f–h) Local stress distribution and atomistic configurations at the connection region between CNT and graphene in rebar graphene model. Heptagons with high stress concentration (g) initiate a local fracture process resulting in either CNT breaking (f) or graphene fracture (h).

shown that the heptagon rings are weak spots for bond breaking in graphene, and our simulations demonstrate that both failure modes, CNT breaking (Figure 6f) or graphene fracture (Figure 6h), initiate at these heptagon rings.[39,44] However, regarding the competing of the two local failure modes, no dominant trend is observed in the simulations. This is consistent with the experimental observation of both CNT pull-out and graphene bridging. It should be pointed out that the detailed atomistic configurations around the connection of CNTs and graphene layer remain unknown in experiments and the simulation model adopted here may still be different from the reality. Further advanced experimental observation and systematic simulations about the connection spots in rebar graphene may unveil more details about these failure modes to tune the bridging mechanism and are left for future study.

MD simulations also show that the CNTs in rebar graphene could deflect the crack path through daughter crack initiation and coarsening and crack bridging. For purposes of comparison, we simulated crack propagation in pristine graphene along zigzag direction using MD as well. As shown in Figure 7a, the crack propagates along a straight line in pristine graphene leaving smooth crack surfaces behind, which is consistent with previous studies.[1] However, in rebar graphene, for example, when the CNTs are oriented inclined with an angle to the initial crack path, as shown in Figure 6b for the sample with inclined CNT pattern, a series of effective bridging events happen along the CNT distribution direction, resulting in the deflection of the crack path during the propagation, which further enhances the fracture energy of rebar graphene (Figure 7c) (see Movie S2 in Supporting Information). The detailed crack defection mechanisms demonstrated in this example are daughter crack initiation and crack coarsening. As shown in Figure 7d, the connections between CNTs and graphene often suffer high stress concentration, and daughter cracks can initiate at these spots. Later, these secondary cracks coarsen and merge into the main crack, achieving a small "jump over" of the crack path (Figure 7e). A sequence of such interaction could deflect the crack path away from the original direction (Figure 7b). Another crack deflection mechanism in rebar graphene is crack bridging. As shown in Figure 7f, strong CNT bridging in a rebar graphene sample with a random staggered pattern of CNTs can also deflect the crack path.

To unveil more details of fracture process in rebar graphene, uniaxial tension tests are performed in rebar graphene strips with a random CNT pattern (Figure 5f). Without an initial edge crack, multiple cracks initiate at different locations, propagate, and interact with each other, resulting in a rich variety of crack initiation and propagation processes (see Movies S3 and S4 in Supporting Information). Figure 7f–i shows that CNT bridging, CNT pulling out/fracture, crack deflection, and graphene bridging are all captured by the simulation, and finally a zigzag crack path forms in the sample, which are consistent with the experimental observation in Figure 4 and further validate the hypothesized toughening mechanisms of rebar graphene in a qualitative way.

DOI: 10.1021/acsnano.8b02311
ACS Nano 2018, 12, 7901–7910

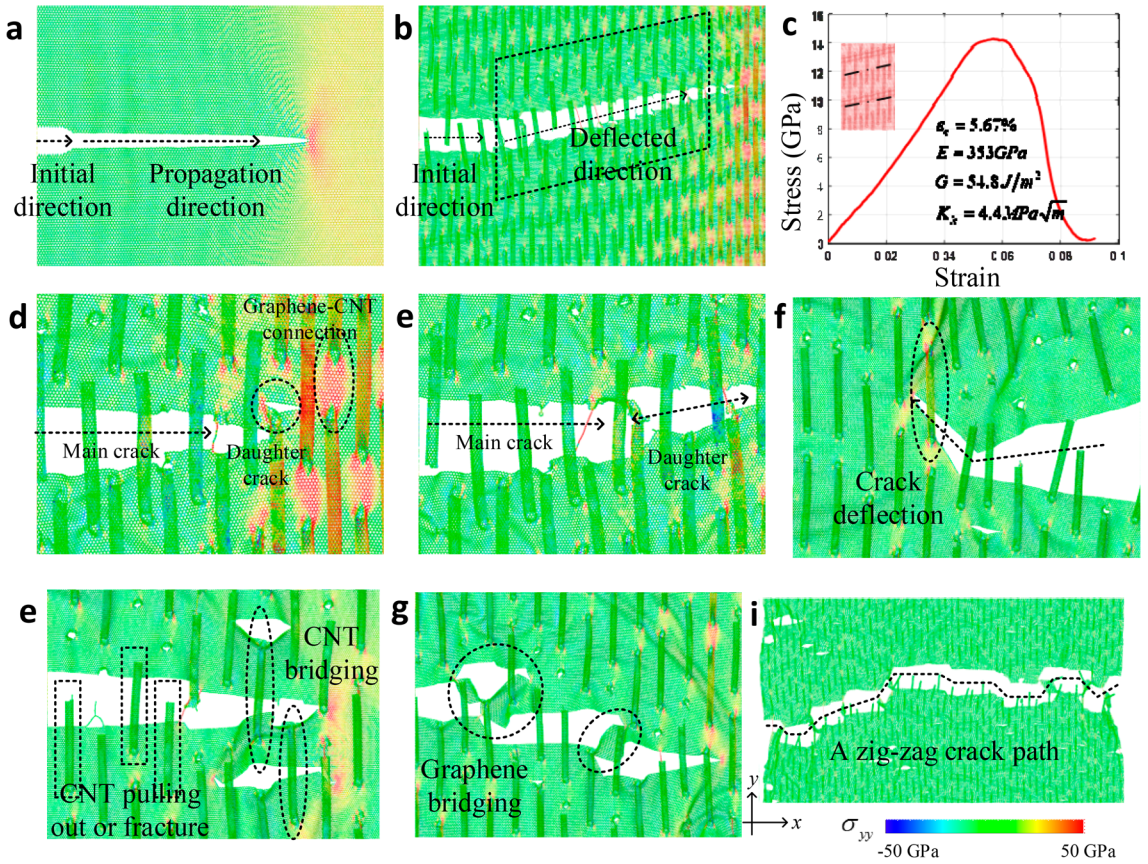

Figure 7. MD simulations of toughening mechanisms in rebar graphene samples. (a) MD simulation of crack propagation in pristine graphene. A straight crack path with smooth crack surfaces are observed. (b, c) MD simulation of crack propagation in a rebar graphene with an inclined staggered distribution of CNTs. The initial horizontal crack is deflected due to the bridging and breaking of a series of CNTs along the inclined direction. A more than a 4-fold enhancement of fracture energy is achieved compared with graphene in MD. (d, e) One step in crack deflection through daughter crack initiation (d) and crack coarsening (e). (f) Crack deflection through strong bridging in a rebar graphene with random staggered CNT pattern. (f–h) MD simulation of uniaxial tension test of a rebar graphene sample with a random staggered CNT pattern. CNT bridging, pulled out or fractured CNTs, crack defection, and graphene bridging are observed during the fracture process, and finally a zigzag crack path cuts through the whole strip.

Due to these novel toughening mechanisms activated in rebar graphene, the fracture toughness measured in MD simulation also shows obvious enhancement. As a comparison, for pristine graphene, we obtained a fracture energy of 11.9 J/m^2 and a critical SIF of 3.5 MPa·m$^{1/2}$ using MD simulation, which is in good agreement with previous study.[1] The rebar graphene model with an inclined staggered pattern of CNTs discussed above shows a fracture energy of 54.8 J/m^2 and a critical SIF of 4.4 MPa·m$^{1/2}$ which achieves a more than 4-fold enhancement in fracture energy.

We also note that the experimental measured value of the critical SIF of rebar graphene reaches an average of 10.50 ± 5.73 MPa·m$^{1/2}$, which is still relatively larger than the simulation results. Qualitatively this discrepancy could be related to the following factors. Due to the limitation of current computational power, the rebar graphene models adopted in MD simulations are considerably smaller than those in real experiments. Correspondingly, the length of CNTs and the complexity of the CNT networks are all reduced and simplified to adjust to the available simulation size. Quantitatively, this scaling down could limit the effect of toughening mechanisms, reduce the size of the processing zone surrounding the crack tip, and lead to an underestimated fracture resistance. What's more, under current experimental condition, the detailed observation of the distribution of the CNT network and the atomistic configurations of the connections between CNTs and graphene layer in rebar graphene remain unknown. There could be different distribution patterns and connection configurations in the experimental samples. As demonstrated in current MD simulations, the CNT network distributions and the defect structure at the connections could affect the toughening mechanisms directly and alter the fracture toughness quantitively. For future study, it is important to combining the advanced experimental observation with MD simulations to construct a quantitative relation between the toughness enhancement and rebar graphene structures.

The previous study demonstrates that the fracture toughness of graphene is only 4.0 MPa·m$^{1/2}$,[1] which suggests that graphene is a typical brittle material. Considering that graphene has a great potential in building flexible devices, in case of resisting mechanical failure, graphene-like materials with higher fracture toughness is in need. Rebar graphene is the graphene toughened by CNTs. The measured fracture toughness is over twice higher than that of pristine graphene. Such promising fracture toughness would make rebar graphene find more practical applications. For example, rebar graphene could be a very good candidate material for flexible transparent conductive electrodes.[40] In flexible electronics, once the electrode is under tension, compression, and twisting, the mechanical behaviors of electrode materials will dominate the

DOI: 10.1021/acsnano.8b02311
ACS Nano 2018, 12, 7901–7910

reliability and stability of the device. Also, the rebar graphene can be used to fabricate 3D rebar graphene foams, which have demonstrated stable performance as a highly porous electrode in lithium-ion capacitors.[40] Another significance of our work is that through the measurement and study of fracture toughness enhancement in rebar graphene, materials with exceptional mechanical performance might be discovered and designed in the future. For example, the unveiled toughening mechanisms in rebar graphene may be applied to design and engineer other tough 2D material systems as hybrids of 2D planar sheets and 1D nanotubes, like rebar hexagonal-boron nitride[45] and even rebar transition-metal dichalcogenides.

CONCLUSIONS

In conclusion, we have performed quantitative *in situ* mechanical tests and numerical simulations on rebar graphene in comparison with similar tests done on pristine graphene and determined toughening mechanisms of the embedded CNTs. Such tests and study are imperative to understanding and enhancing mechanical properties of 2D materials before their integration into robust electronic devices. The CNTs toughen the graphene as seen by the increased average SIF values obtained. This is further seen in a comparison of the nature of the crack propagations in graphene and rebar graphene. Graphene fractures in a linear, brittle manner where graphene rebar displays a zigzag fracture surface, guided and redirected by the embedded CNTs. The creation of this hybrid graphene material opens the door to many other 2D composites that can be mechanically tailored to the needs of their flexible device applications.

METHODS

Synthesis of Rebar Graphene. The rebar graphene was prepared similarly to the previous reports.[4,32] Specifically, single-walled CNTs (SWCNTs) (7 mg) were dispersed together with Pluronic 127 (10 mg, Sigma-Aldrich) in DI water (10 mL) and then tip sonicated (Misonix Sonicator 3000) at 80 W for 20 min to generate a homogeneous SWCNT solution. A 25 μm-thick 10 cm × 10 cm Cu foil (99.8% purity, Alfa Aesar) was pretreated using the electrochemical polishing method.[4] The pretreated Cu foil was cut into 1 cm × 1 cm pieces and coated with the SWCNT solution by spin-coating at 1000 rpm for 30 s for 15 times. The Cu foils were then loaded into a CVD furnace at 1070 °C and annealed with 500 sccm H_2 at 7 Torr for 5 min, and then an additional 5 sccm CH_4 was introduced for 15 min to promote graphene growth.

Dry Transfer Technique. Sample preparation has proven to be the biggest challenge in mechanically testing 2D materials. Our testing device cannot contact liquid since it will damage the suspended working layer of the device, resulting in the need to develop a "dry" transfer method. Figure 2a–d schematically shows the transfer technique developed in this study.[3] The synthesized rebar graphene was spin coated with poly(methyl methacrylate) (PMMA) with a layer thickness of about 200–300 nm and heated on a hot plate at 180 °C for 1 min to ensure adhesion between the rebar graphene and PMMA. The copper growth substrate was etched away using ammonium perchlorate. The floating film of rebar graphene and PMMA was fished out of the etchant using a silicon wafer and washed and transferred onto a copper transmission electron microscope (TEM) grid. A fine-tungsten micromanipulator probe was used to cut the desired area of PMMA-coated rebar graphene and to carefully load the 2D material over the test section of the micromechanical device under an optical microscope. The film adheres to the silicon device through van der Waals forces facilitated by heat treatment. The PMMA was then annealed in 90% nitrogen and 10% hydrogen mixed CVD tube furnace (Lindbergh/Blue M, Thermo Scientific). The temperature was raised to 400 °C over the course of 1.5 h and held at 400 °C for 2 h with continuous flow of the gas mixture under atmospheric pressure. Once the devices were annealed and naturally cooled to ambient temperature, a focused ion beam (FIB, Helios 660) was used to cut the sample into final testing geometry. The FIB was also used to introduce a precrack into the sample for fracture toughness measurements. The devices were then glued to an SEM stub using crystal bond.

Mechanical Testing of Rebar Graphene. Quantitative *in situ* tensile testing was performed using an Agilent inSEM nanoindenter to actuate the micromechanical device. Load and displacement were measured in real time during the tensile test being performed. With known sample geometrical parameters, mechanical properties such as Young's modulus and failure stress/strain can be determined. Video footages of the tests were also recorded to ensure validity of each test.

***In Situ* TEM Tensile Testing of Rebar Graphene.** A custom TEM holder and an aluminum stage were recently designed and built in house.[1] Rebar graphene samples were transferred onto a thermally actuated silicon-based inTEM microdevice following the same dry transfer technique. The inTEM device was firmly attached to the stage using Crystalbond adhesive. Two Au microwires with 25 μm diameter were bonded to the Au pad on the TEM device and the copper strip which connects to the outside electrical circuit. Two sets of inclined beams in the TEM device are driven by Joule heating supplied by Keithley Digital Meter with voltage ranging from 0 to 8 V to realize uniaxial tensile test in TEM (JEOL 2100 F). Details about the inTEM microdevice, stage, holder, and rebar graphene suspended over the inTEM microdevice can be found in the Supporting Information Figure S1.

MD Simulations of Rebar Graphene. MD simulations of rebar graphene structure were carried out *via* large-scale atomic/molecular massively parallel simulator.[41] Visualization was processed *via* software package Ovito.[42] The interatomic forces were described by the adaptive intermolecular reactive empirical bond order (AIREBO) potential.[43] To avoid a nonphysical posthardening behavior known to exist for the AIREBO potential, the smaller cutoff distance in the switching function of AIREBO was taken to be 2.0 Å, as suggested by previous studies.[6,16,44,45]

ASSOCIATED CONTENT

Supporting Information

The Supporting Information is available free of charge on the ACS Publications website at DOI: 10.1021/acsnano.8b02311.

Microdevice and holder for *in situ* tensile test in TEM; strength comparison between rebar graphene and CVD-grown graphene; spread of the experimental measured strength and stiffness of rebar graphene; effect of the geometry and distribution of CNTs on the toughness enhancement (PDF)

Movie S1: Edge crack propagation in a strip of rebar graphene with a horizontal CNT pattern (AVI)

Movie S2: Edge crack propagation in a strip of rebar graphene with an inclined CNT pattern (AVI)

Movie S3: Uniaxial tension of a strip of rebar graphene with a random CNT pattern (AVI)

Movie S4: Uniaxial tension of a strip of rebar graphene with a random CNT pattern. A circular hole is added to represent the possible defect introduced during transferring in experiments (AVI)

AUTHOR INFORMATION

Corresponding Author

*E-mail: jlou@rice.edu.

ORCID

Yilun Li: 0000-0002-0750-2228

Qing Chen: 0000-0002-7919-5159

DOI: 10.1021/acsnano.8b02311
ACS Nano 2018, 12, 7901–7910

James M. Tour: 0000-0002-8479-9328

Author Contributions

○These authors contributed equally.

Notes

The authors declare no competing financial interest.

ACKNOWLEDGMENTS

The authors gratefully acknowledge the Welch Foundation grant C-1716, the Air Force Office of Scientific Research MURI grant FA9550-12-1-0035 (for sample preparations and qualitative in TEM studies), and the US Department of Energy, Office of Basic Energy Sciences under grant number DE-SC0018193 (for quantitative in SEM studies). J.L., Q.C., and X.L. were also supported by the National Natural Science Foundation of China (grant no. 11528407). B.N. and H.G. acknowledge support from the National Science Foundation (grant CMMI-1634492).

REFERENCES

(1) Zhang, P.; Ma, L. L.; Fan, F. F.; Zeng, Z.; Peng, C.; Loya, P. E.; Liu, Z.; Gong, Y. J.; Zhang, J. N.; Zhang, X. X.; Ajayan, P. M.; Zhu, T.; Lou, J. Fracture Toughness of Graphene. *Nat. Commun.* **2014**, *5*, 3782.

(2) Lee, G. H.; Cooper, R. C.; An, S. J.; Lee, S.; van der Zande, A.; Petrone, N.; Hammerberg, A. G.; Lee, C.; Crawford, B.; Oliver, W.; et al. High-Strength Chemical-Vapor-Deposited Graphene and Grain Boundaries. *Science* **2013**, *340*, 1073−1076.

(3) Yang, Y. C.; Li, X.; Wen, M.; Hacopian, E.; Chen, W.; Gong, Y.; Zhang, J.; Li, B.; Zhou, W.; Ajayan, P. M.; Chen, Q.; Zhu, T.; Lou, J. Brittle Fracture of 2D $MoSe_2$. *Adv. Mater.* **2017**, *29*, 1604201.

(4) Yan, Z.; Peng, Z.; Casillas, G.; Lin, J.; Xiang, C.; Zhou, H.; Yang, Y.; Ruan, G.; Raji, A. R. O.; Samuel, E. L.; Hauge, R. H.; Yacaman, M. J.; Tour, J. M. Rebar Graphene. *ACS Nano* **2014**, *8*, 5061−5068.

(5) Geim, A. K.; Novoselov, K. S. The Rise of Graphene. *Nat. Mater.* **2007**, *6*, 183−191.

(6) Zhang, T.; Li, X.; Kadkhodaei, S.; Gao, H. Flaw Insensitive Fracture in Nanocrystalline Graphene. *Nano Lett.* **2012**, *12*, 4605−4610.

(7) Zhao, H.; Min, K.; Aluru, N. Size and Chirality Dependent Elastic Properties of Graphene Nanoribbons under Uniaxial Tension. *Nano Lett.* **2009**, *9*, 3012−3015.

(8) Bolotin, K. I.; Sikes, K.; Jiang, Z.; Klima, M.; Fudenberg, G.; Hone, J.; Kim, P.; Stormer, H. Ultrahigh Electron Mobility in Suspended Graphene. *Solid State Commun.* **2008**, *146*, 351−355.

(9) Balandin, A. A.; Ghosh, S.; Bao, W.; Calizo, I.; Teweldebrhan, D.; Miao, F.; Lau, C. N. Superior Thermal Conductivity of Single-Layer Graphene. *Nano Lett.* **2008**, *8*, 902−907.

(10) Dean, C. R.; Young, A. F.; Meric, I.; Lee, C.; Wang, L.; Sorgenfrei, S.; Watanabe, K.; Taniguchi, T.; Kim, P.; Shepard, K. L.; et al. Boron Nitride Substrates for High-Quality Graphene Electronics. *Nat. Nanotechnol.* **2010**, *5*, 722−726.

(11) Novoselov, K. S.; Geim, A. K.; Morozov, S. V.; Jiang, D.; Zhang, Y.; Dubonos, S. V.; Grigorieva, I. V.; Firsov, A. A. Electric Field Effect in Atomically Thin Carbon Films. *Science* **2004**, *306*, 666−669.

(12) Lee, C.; Wei, X.; Kysar, J. W.; Hone, J. Measurement of the Elastic Properties and Intrinsic Strength of Monolayer Graphene. *Science* **2008**, *321*, 385−388.

(13) Gómez-Navarro, C.; Burghard, M.; Kern, K. Elastic Properties of Chemically Derived Single Graphene Sheets. *Nano Lett.* **2008**, *8*, 2045−2049.

(14) Balandin, A. A. Thermal Properties of Graphene and Nanostructured Carbon Materials. *Nat. Mater.* **2011**, *10*, 569−581.

(15) Lee, C.; Wei, X.; Li, Q.; Carpick, R.; Kysar, J. W.; Hone, J. Elastic and Frictional Properties of Graphene. *Phys. Status Solidi B* **2009**, *246*, 2562−2567.

(16) Terdalkar, S. S.; Huang, S.; Yuan, H.; Rencis, J. J.; Zhu, T.; Zhang, S. Nanoscale Fracture in Graphene. *Chem. Phys. Lett.* **2010**, *494*, 218−222.

(17) Shekhawat, A.; Ritchie, R. O. Toughness and Strength of Nanocrystalline Graphene. *Nat. Commun.* **2016**, *7*, 10546.

(18) Faccio, R.; Denis, P. A.; Pardo, H.; Goyenola, C.; Mombrú, A. W. Mechanical Properties of Graphene Nanoribbons. *J. Phys.: Condens. Matter* **2009**, *21*, 285304.

(19) Claussen, N. Fracture Toughness of Al_2O_3 with an Unstabilized ZrO_2 Dispersed Phase. *J. Am. Ceram. Soc.* **1976**, *59*, 49−51.

(20) George, R.; Kashyap, K.; Rahul, R.; Yamdagni, S. Strengthening in Carbon Nanotube/Aluminium (CNT/Al) Composites. *Scr. Mater.* **2005**, *53*, 1159−1163.

(21) Cha, S. I.; Kim, K. T.; Arshad, S. N.; Mo, C. B.; Hong, S. H. Extraordinary Strengthening Effect of Carbon Nanotubes in Metal-Matrix Nanocomposites Processed by Molecular-Level Mixing. *Adv. Mater.* **2005**, *17*, 1377−1381.

(22) Yang, Y. C.; Rigdon, W.; Huang, X.; Li, X. Enhancing Graphene Reinforcing Potential in Composites by Hydrogen Passivation Induced Dispersion. *Sci. Rep.* **2013**, *3*, 2086.

(23) Stankovich, S.; Dikin, D. A.; Dommett, G. H.; Kohlhaas, K. M.; Zimney, E. J.; Stach, E. A.; Piner, R. D.; Nguyen, S. T.; Ruoff, R. S. Graphene-Based Composite Materials. *Nature* **2006**, *442*, 282−286.

(24) Ramanathan, T.; Abdala, A.; Stankovich, S.; Dikin, D.; Herrera-Alonso, M.; Piner, R.; Adamson, D.; Schniepp, H.; Chen, X.; Ruoff, R.; et al. Functionalized Graphene Sheets for Polymer Nanocomposites. *Nat. Nanotechnol.* **2008**, *3*, 327−331.

(25) Potts, J. R.; Dreyer, D. R.; Bielawski, C. W.; Ruoff, R. S. Graphene-Based Polymer Nanocomposites. *Polymer* **2011**, *52*, 5−25.

(26) Xiong, D. B.; Cao, M.; Guo, Q.; Tan, Z.; Fan, G.; Li, Z.; Zhang, D. Graphene-and-Copper Artificial Nacre Fabricated by a Preform Impregnation Process: Bioinspired Strategy for Strengthening-Toughening of Metal Matrix Composite. *ACS Nano* **2015**, *9*, 6934−6943.

(27) Chen, Z.; Ren, W.; Gao, L.; Liu, B.; Pei, S.; Cheng, H. M. Three-Dimensional Flexible and Conductive Interconnected Graphene Networks Grown by Chemical Vapour Deposition. *Nat. Mater.* **2011**, *10*, 424−428.

(28) Wang, D.; Choi, D.; Li, J.; Yang, Z.; Nie, Z.; Kou, R.; Hu, D.; Wang, C.; Saraf, L. V.; Zhang, J.; et al. Self-Assembled TiO_2-Graphene Hybrid Nanostructures for Enhanced Li-Ion Insertion. *ACS Nano* **2009**, *3*, 907−914.

(29) Jung, G.; Qin, Z.; Buehler, M. J. Molecular Mechanics of Polycrystalline Graphene with Enhanced Fracture Toughness. *Extreme Mech. Lett.* **2015**, *2*, 52−59.

(30) Geim, A. K.; Grigorieva, I. V. van der Waals Heterostructures. *Nature* **2013**, *499*, 419−425.

(31) Levendorf, M. P.; Kim, C. J.; Brown, L.; Huang, P. Y.; Havener, R. W.; Muller, D. A.; Park, J. Graphene and Boron Nitride Lateral Heterostructures for Atomically Thin Circuitry. *Nature* **2012**, *488*, 627−632.

(32) Li, Y.; Peng, Z.; Larios, E.; Wang, G.; Lin, J.; Yan, Z.; Ruiz-Zepeda, F.; José-Yacamán, M.; Tour, J. M. Rebar Graphene from Functionalized Boron Nitride Nanotubes. *ACS Nano* **2015**, *9*, 532−538.

(33) Zhu, Y.; Li, L.; Zhang, C.; Casillas, G.; Sun, Z.; Yan, Z.; Ruan, G.; Peng, Z.; Raji, A. R. O.; Kittrell, C.; et al. A Seamless Three-Dimensional Carbon Nanotube Graphene Hybrid Material. *Nat. Commun.* **2012**, *3*, 1225.

(34) Gojny, F.; Wichmann, M.; Köpke, U.; Fiedler, B.; Schulte, K. Carbon Nanotube-Reinforced Epoxy-Composites: Enhanced Stiffness and Fracture Toughness at Low Nanotube Content. *Compos. Sci. Technol.* **2004**, *64*, 2363−2371.

(35) Yang, Y. C.; Kim, N. D.; Varshney, V.; Sihn, S.; Li, Y.; Roy, A. K.; Tour, J. M.; Lou, J. *In Situ* Mechanical Investigation of Carbon Nanotube-Graphene Junction in Three-Dimensional Carbon Nanostructures. *Nanoscale* **2017**, *9*, 2916−2924.

(36) Yang, Y. C.; Chen, W.; Hacopian, E.; Dong, P.; Sun, A.; Ci, L.; Lou, J. Unveil the Size-Dependent Mechanical Behaviors of Individual

DOI: 10.1021/acsnano.8b02311
ACS Nano 2018, 12, 7901−7910

CNT/SiC Composite Nanofibers by *In Situ* Tensile Tests in SEM. *Small* **2016**, *12*, 4486−4491.
(37) Ganesan, Y.; Lu, Y.; Peng, C.; Lu, H.; Ballarini, R.; Lou, J. Development and Application of a Novel Microfabricated Device for the *In Situ* Tensile Testing of 1-D Nanomaterials. *J. Microelectromech. Syst.* **2010**, *19*, 675−682.
(38) Hoover, W. G. Canonical Dynamics: Equilibrium Phase-Space Distributions. *Phys. Rev. A: At., Mol., Opt. Phys.* **1985**, *31*, 1695.
(39) Wei, Y.; Wu, J.; Yin, H.; Shi, X.; Yang, R.; Dresselhaus, M. The Nature of Strength Enhancement and Weakening by Pentagon−Heptagon Defects in Graphene. *Nat. Mater.* **2012**, *11*, 759−763.
(40) Sha, J.; Salvatierra, R. V.; Dong, P.; Li, Y.; Lee, S. K.; Wang, T.; Zhang, C.; Zhang, J.; Ji, Y.; Ajayan, P. M.; Lou, J.; Zhao, N. Q.; Tour, J. M. Three-Dimensional Rebar Graphene. *ACS Appl. Mater. Interfaces* **2017**, *9*, 7376−7384.
(41) Plimpton, S. Fast Parallel Algorithms for Short-Range Molecular Dynamics. *J. Comput. Phys.* **1995**, *117*, 1−19.
(42) Stukowski, A. Visualization and Analysis of Atomistic Simulation Data with OVITO−the Open Visualization Tool. *Modell. Simul. Mater. Sci. Eng.* **2010**, *18*, 015012.
(43) Stuart, S. J.; Tutein, A. B.; Harrison, J. A. A Reactive Potential for Hydrocarbons with Intermolecular Interactions. *J. Chem. Phys.* **2000**, *112*, 6472−6486.
(44) Zhang, T.; Li, X.; Gao, H. Designing Graphene Structures with Controlled Distributions of Topological Defects: A Case Study of Toughness Enhancement in Graphene Ruga. *Extreme Mech. Lett.* **2014**, *1*, 3−8.
(45) Shenderova, O.; Brenner, D.; Omeltchenko, A.; Su, X.; Yang, L. Atomistic Modeling of the Fracture of Polycrystalline Diamond. *Phys. Rev. B: Condens. Matter Mater. Phys.* **2000**, *61*, 3877.

DOI: 10.1021/acsnano.8b02311
ACS Nano 2018, 12, 7901−7910